Kinetics and Mechanism of Aqueous Chemical Synthesis of $BaTiO_3$ Particles

Andrea Testino,[†] Maria Teresa Buscaglia,[‡] Vincenzo Buscaglia,*[,‡] Massimo Viviani,[‡] Carlo Bottino,[‡] and Paolo Nanni[†]

Institute for Energetics and Interphases, Department of Genoa, National Research Council, I-16149 Genoa, Italy, and Department of Process and Chemical Engineering, University of Genoa, I-16129 Genoa, Italy

Received September 17, 2003. Revised Manuscript Received November 24, 2003

A systematic kinetic investigation on the chemical synthesis of $BaTiO_3$ particles from aqueous solutions of $BaCl_2$ and $TiCl_4$ at $T < 100$ °C and at pH 14 has been performed. Initially, a viscous suspension of a Ti-rich gel phase is obtained at room temperature. Later, formation of $BaTiO_3$ is induced by heating above 70 °C and the gel phase is gradually converted to the crystalline perovskite. The isothermal formation kinetics of $BaTiO_3$ and the evolution of crystal size and particle size during the course of reaction are significantly influenced by temperature, concentration, and barium-to-titanium ratio of the solution. The early stages of reaction (yield < 1%) are dominated by primary nucleation, and slow formation of single nanocrystals of $BaTiO_3$ was observed by HRTEM. At a later stage, formation of polycrystalline particles occurs by secondary nucleation of $BaTiO_3$ on the surface of already existing crystals. During this stage, the reaction rate increases by 1 order of magnitude. When the yield exceeds 50%, nucleation becomes less important and the reaction is dominated by growth. Final particles have a diameter in the range 0.3−1.6 μm, depending on the processing parameters.

1. Introduction

Barium titanate, $BaTiO_3$, is a ferroelectric ceramic massively used in electric and electronic applications. As a dielectric, it is utilized in multilayer ceramic capacitors (MLCCs) and for embedded capacitance in printed circuit boards. Recent developments in microelectronics and communication have led to the miniaturization of MLCCs. To achieve this goal and to make the next step forward, powders with improved quality and small and uniform size (<300 nm) are required.[1]

Many chemical methods have been proposed for the synthesis of high-quality $BaTiO_3$ powders.[2] Among them, the hydrothermal route has some advantages because it leads directly to fine, pure, crystalline powders at relatively low temperatures without the need of a further thermal treatment. The hydrothermal process is generally carried out by suspending TiO_2 particles or a TiO_2 gel in an aqueous $Ba(OH)_2$ solution and then autoclaving at 150−300 °C. Thermodynamic modeling of the $Ti-Ba-H_2O-CO_2$ system[3] has been used to assess the conditions corresponding to the quantitative formation of $BaTiO_3$. In the absence of CO_2 and at pH >12, $BaTiO_3$ is the stable phase over a wide range of barium concentrations. The calculated stability diagrams have also shown that quantitative formation of $BaTiO_3$ is possible even at temperatures <100 °C. Therefore, synthesis of $BaTiO_3$ using more conventional chemical precipitation processes has also been explored.[4−8]

The size distribution of the particles that grow from solution depends, in general, on the rates of nuclei formation and crystallite growth. Crystal agglomeration can also contribute substantially the overall particle growth process.[9−10] The relative importance of nucleation and growth is determined by the supersaturation of the solution. In turn, supersaturation is very sensitive to temperature, concentration, and mixing conditions. Despite the large potential interest, there is scanty information available on the influence of the above parameters on the formation kinetics of $BaTiO_3$ particles.[11−14] The evolution of particle morphology during hydrothermal synthesis was reported by several

* To whom correspondence should be addressed. E-mail: v.buscaglia@ge.ieni.cnr.it.
[†] University of Genoa.
[‡] National Research Council.

(1) Rae, A.; Chu, M.; Ganine, V. In *Ceramic Transactions Dielectric Ceramic Materials*; Nair, K. M., Bhalla, A. S., Eds.; The American Ceramic Society: Westerville, OH, 1999; Vol. 100, p 1. (b) Venigalla, S. *Am. Ceram. Soc. Bull.* **2001**, *6*, 63.
(2) Nanni, P.; Viviani, M.; Buscaglia, V. In *Handbook of Low and High Dielectric Constant Materials and Their Applications*; Nalwa, H. S., Ed.; Academic Press: San Diego, CA, 1999; Vol. 1, p 429.
(3) Lencka, M. M.; Riman, R. E. *Chem. Mater.* **1993**, *5*, 61. (b) Lencka, M. M.; Riman, R. E. *Ferroelectrics* **1994**, *151*, 159.
(4) Kiss, K.; Magder, J.; Vukasovich, M. S.; Lockhart, R. J. *J. Am. Ceram. Soc.* **1966**, *49*, 291.
(5) Her, Y.-S.; Matijevic, E.; Chon, M. C. *J. Mater. Res.* **1995**, *10*, 3106. (b) Her, Y.-S.; Lee, S.-H.; Matijevic, E. *J. Mater. Res.* **1996**, *11*, 156.
(6) Leoni, M.; Viviani, M.; Nanni, P.; Buscaglia, V. *J. Mater. Sci. Lett.* **1996**, *15*, 1302.
(7) Kumar, V. *J. Am. Ceram. Soc.* **1999**, *82*, 2580.
(8) Grohe, B.; Miehe, G.; Wegner, G. *J. Mater. Res.* **2001**, *16*, 1901.
(9) Dirksen, J. A.; Ring, T. A. *Chem. Eng. Sci.* **1991**, *46*, 2389.
(10) Zukoski, C. F.; Rosenbaum, D. F.; Zamora, P. C. *Chem. Eng. Res. Des.* **1996**, *74A*, 723. (b) Van Hyning, D. L.; Klemperer, W. G.; Zukoski, C. F. *Lamgmuir* **2001**, *17*, 3128.
(11) Hertl, W. *J. Am. Ceram. Soc.* **1988**, *71*, 879.

10.1021/cm031130k CCC: $27.50
Published on Web 03/23/2004

Table 1. Summary of Precipitation Experiments and Properties of Final Powders[a]

expt	[Ba] (mol dm^{-3})	[Ba]/[Ti] gel phase	duration (min)	final yield (%)	$t_{1/2}$[b] (min)	final d_{50} (μm)	$(d_{90} - d_{10})/d_{50}$	final d_{BET} (μm)	final d_{XRD} (μm)
					82 °C				
1	0.035	0.63	1320	92	185	2.2[c]	1.0		>0.3
2	0.044	0.63	150	100	47.5	0.86	0.75	0.29	0.26
3	0.052	0.66	66	100	13.4	0.55	0.51	0.25	0.22
4	0.070	0.64	48	100	2.6	0.36	0.49	0.20	0.22
5	0.121		30	100	<1	0.28	0.56	0.16	0.10
6	0.045	0.63	37	100	8.5	0.51	0.47	0.24	0.21
7	0.047	0.64	41	100	4.5	0.49	0.49	0.25	0.27
					92 °C				
8	0.023	0.57	270	91	62	1.57	0.96		>0.3
9	0.029	0.56	65	93	6.9	0.77	0.61	0.22	0.14
10	0.035	0.53	34	100	6.1	0.57	0.58	0.21	0.21
11	0.0405	0.53	14.5	100	3.8	0.47	0.69	0.19	0.12
12	0.059		30	100	<1	0.36	0.46	0.18	0.10

[a] For expts 1−5 and 8−12, $R = 1.11$. For expt 6, $R = 1.155$. For expt 7, $R = 1.2$. R is the [Ba]/[Ti] ratio in the reactor. [b] Half-transformation time for formation of $BaTiO_3$. [c] d_{50} is 1.38 μm after 270 min.

groups,[13−24] but the observations were mainly qualitative.

Analysis of the above-cited literature shows that many fundamental aspects of the formation of $BaTiO_3$ particles from solution are not yet well defined. In general, the formation rate of $BaTiO_3$ increases and the particle size decreases with increasing barium concentration, but these dependencies were never studied on a systematic basis. The effect of temperature is uncertain. The particles are often polycrystalline, but it is unclear whether this is a consequence of secondary nucleation or originates from colloidal aggregation of smaller crystals. In any case, heterogeneous nucleation is reported to be an important factor at the early stages of reaction. Tendency to formation of dendritic particles was also observed when the barium concentration is decreased.

The study described here was aimed to gain a better understanding of the formation of barium titanate particles from dilute (≤0.1 M) aqueous metal chloride solutions at temperatures <100 °C. Synthesis of $BaTiO_3$ particles was carried out according to the overall reaction

$$BaCl_2(aq) + TiCl_4(aq) + 6NaOH(aq) \rightarrow BaTiO_3(s) + 6NaCl(aq) + 3H_2O(l) \quad (1)$$

where (aq) denotes a salt in an aqueous solution. According to our observations, reaction 1 is rather fast at $T \geq 80$ °C and cation concentration >0.1 mol dm^{-3}, and formation of a white $BaTiO_3$ precipitate can be readily observed. However, at lower concentration, the reaction proceeds in two steps: (i) initial, rapid formation of an amorphous Ti-rich gel phase and (ii) slower reaction between the gel phase and the Ba^{2+} ions left in solution with formation of crystalline $BaTiO_3$ particles. While step (i) is very fast at any temperature, step (ii) is hindered below ≈70 °C. The isothermal crystallization kinetics and the evolution of morphology, crystallite size, and particle size were determined as a function of concentration at two different temperatures. The influence of the barium-to-titanium ratio was investigated for a given combination of temperature and Ti concentration.

2. Experimental Section

2.1. Synthesis of $BaTiO_3$. To obtain reproducible results corresponding to a well-defined condition, precipitation experiments were carried out by premixing the reactant solutions at room temperature, where formation of $BaTiO_3$ is kinetically inhibited, and then heating the resulting gel suspension to the reaction temperature. Several precipitation experiments (see Table 1) were performed in a 500 mL vessel using ≈250 mL of an aqueous solution of $TiCl_4$ (Acros, 99.9%) and $BaCl_2{\cdot}2H_2O$ (Aldrich, 99.9%). The chloride solution was quickly mixed (20 s) with the same volume of a NaOH solution with immediate formation of a highly viscous, gelatinous suspension of a Ti-rich gel phase. The concentration of the NaOH solution was that required to have [OH$^-$] = 1 mol dm^{-3} after quantitative precipitation of $BaTiO_3$, according to reaction 1. The experiments were conducted at two different temperatures, 82 and 92 °C, and the barium concentration in the reactor (i.e. the concentration referred to the total volume after mixing of the reactant solutions) was varied from 0.02 to 0.12 mol dm^{-3}. Unless otherwise stated, the [Ba]/[Ti] molar ratio, R, in the solution was 1.11. The vessel was then closed, heated, and kept at constant temperature with stirring. The closed environment avoids formation of $BaCO_3$. The temperature inside the reactor was measured by means of a Pt100 sensor. Progressive formation of crystalline $BaTiO_3$ occurs during aging. The transformation was visually indicated by the transition from a translucent viscous medium to a white and opaque suspension. The head of the reactor was equipped with 12 plastic (PEEK) tubes and valves. Each tube was connected to a

(12) Vivekanandan, R.; Philip, S.; Kutty, T. R. N. *Mater. Res. Bull.* **1986**, *22*, 99. (b) Kutty, T. R. N.; Padmini, P. *Mater. Chem. Phys.* **1995**, *39*, 200.
(13) Eckert, J. O., Jr.; Hung-Houston, C. C.; Gersten, B. L.; Lencka, M. M.; Riman, R. E. *J. Am. Ceram. Soc.* **1996**, *79*, 2929.
(14) Moon, J.; Suvaci, E.; Morrone, A.; Costantino, S. A.; Adair, J. H. *J. Eur. Ceram. Soc.* **2003**, *23*, 2153.
(15) Hennings, D.; Rosenstein, G.; Schreinemacher, H. *J. Eur. Ceram. Soc.* **1991**, *8*, 107.
(16) Dutta, P. K.; Gregg, J. R. *Chem. Mater.* **1992**, *4*, 843. (b) Dutta, P. K.; Asiaie, R.; Akbar, S. A.; Zhu, W. *Chem. Mater.* **1994**, *6*, 1542.
(17) Kumazawa, H.; Annen, S.; Sada, E. *J. Mater. Sci.* **1995**, *30*, 4740.
(18) Chien, A. T.; Speck, J. S.; Lange, F. F.; Daykin, A. C.; Levi, C. G. *J. Mater. Res.* **1995**, *10*, 1784.
(19) Slamovich, E. B.; Aksay, I. A. *J. Am. Ceram. Soc.* **1996**, *79*, 239.
(20) Zhao, L.; Chien, A. T.; Lange, F. F.; Speck, J. S. *J. Mater. Res.* **1996**, *11*, 1325.
(21) Choi, J. Y.; Kim, C. H.; Kim, D. K. *J. Am. Ceram. Soc.* **1998**, *81*, 1353.
(22) Bagwell, R. B.; Sindel, J.; Sigmund, W. *J. Mater. Res.* **1999**, *14*, 1844.
(23) Hu, M. Z.-C.; Kurian, V.; Payzant, E. A.; Rawn, C. J.; Hunt, R. D. *Powd. Technol.* **2000**, *110*, 2.
(24) MacLaren, I.; Ponton, C. B. *J. Eur. Ceram. Soc.* **2000**, *20*, 1267.

syringe on one side and immersed in the suspension on the other side. At given times (time zero corresponds to the instant the temperature reaches the reaction temperature) 20 mL of suspension was collected, cooled, and sealed in small bottles. Each syringe was used only once. The aliquot collected at time zero was used to determine the Ba/Ti ratio in the gel phase. After quantitative precipitation of $BaTiO_3$ (or when conversion attains a constant value), the suspension remaining in the reactor was centrifuged, and the powder was washed and finally freeze-dried.

2.2. Particle Characterization and Measurement of Particle Size Distribution. A 5−10 mL portion of suspension was washed and filtered on a filter paper. The X-ray diffraction (XRD) pattern of the precipitate was collected directly from the surface of the filter after drying with a Philips PW1710 diffractometer (Co Kα radiation). The powder patterns, including (110) and (111) reflections, were recorded in the range 35−50° 2θ using a 2θ step of 0.03° and a sampling time (for each step) up to 60 s for samples containing a small amount of crystalline phase. The crystallite size (d_{XRD}) of $BaTiO_3$ was estimated from the broadening of the (111) XRD peak by means of the Scherrer equation, after correction for instrumental broadening, assuming negligible microstrain broadening. The (*hhh*) reflections are not subjected to splitting during the cubic to tetragonal distortion of the $BaTiO_3$ unit cell. The drawback of using the (111) reflection is its low relative intensity, only 30%. Therefore, for yield values <10%, meaningful crystal size measurements could not be carried out because the signal-to-noise ratio was too low. Since the broadening effect for particles >150 nm is rather small, size measurements of the coarser crystallites may be affected by a large uncertainty. Above 300 nm, broadening is negligible and size measurements are no longer possible. Because of the limitations described above, the crystallite size data should be considered as semiquantitative values.

The number particle size distribution (PSD) was obtained from the measurement of the diameter of ≈1000 particles by a Philips 515 scanning electron microscope (SEM). For this purpose, 5 mL of suspension was centrifuged, and the precipitate was washed and finally treated with a 5% HNO_3 solution to dissolve the gel phase, leaving the $BaTiO_3$ particles. SEM observation before and after the treatment has shown no appreciable variation of particle morphology. Three parameters, d_{10}, d_{50}, and d_{90}, were obtained from the PSD. In general, d_p is the diameter corresponding to the percentage p of particles in the cumulative particle size distribution. The average particle size was defined as the number median diameter (d_{50}) of the PSD.

The powder obtained after completion of reaction was also characterized. The density, ρ, was measured by helium picnometry (model Accupyc 1330, Micromeritics, Norcross, GA). The specific surface area, S_{BET}, was determined by nitrogen physisorption (BET method, model ASAP 2010, Micromeritics, Norcross, GA). The equivalent BET diameter, d_{BET}, was calculated with the formula $d_{BET} = 6/\rho S_{BET}$.

2.3. Determination of the Reaction Kinetics. *Method 1.* A 10 mL portion of suspension was centrifuged and the barium concentration in the supernatant was determined by gravimetric titration as $BaSO_4$. Use of conductometric titration gave equivalent results. The progress of reaction was calculated by the equation

$$\text{yield} = \frac{R([\text{Ba}] - [\text{Ba}]_T) + R_g[\text{Ba}]_T}{(R_g - 1)[\text{Ba}]_T}$$

where [Ba] is the barium concentration in the supernatant, $[Ba]_T$ the total barium concentration, and R_g the Ba/Ti ratio in the gel phase (measured on the suspension withdrawn at time zero), assumed to be constant during the course of reaction. This hypothesis was verified by determining the precipitation kinetics at a barium concentration of 0.035 mol dm^{-3} by a second independent method.

Method 2. The suspension was centrifuged, the precipitate washed, and finally the gel phase was removed by the same treatment adopted for PSD measurement. The $BaTiO_3$ precipitate was finally dissolved using a 3:1 mixture of concentrated HCl and HNO_3, and the amount of barium was determined by gravimetric titration. Although SEM observations showed that the treatment for removal of the gel phase has not an appreciable influence on particle morphology, leaching of barium ions from the surface of $BaTiO_3$ could not be completely avoided and a small correction of the raw kinetic data was required for method 2. This correction was determined from the amount of barium dissolved from a reference $BaTiO_3$ powder prepared with the same methodology and subjected to the same treatment. As shown in Figure 1, the kinetic data obtained by the two methods result to be nearly coincident. However, method 1 was preferred because it is faster and more reliable.

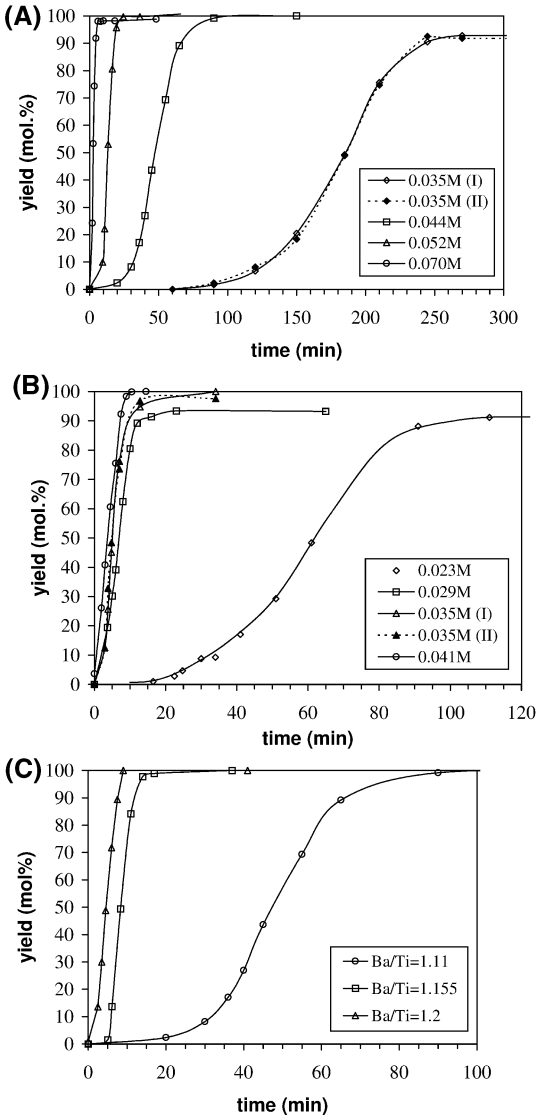

Figure 1. Formation kinetics of crystalline $BaTiO_3$ from aqueous solutions of $BaCl_2$ and $TiCl_4$. The legend of (a) and (b) indicates the barium concentration. (a) At 82 °C and [Ba]/[Ti] = 1.11. (b) At 92 °C and [Ba]/[Ti] = 1.11. (c) At 82 °C and [Ti] = 0.039 mol dm^{-3} for different values of [Ba]/[Ti]. Open symbols represent kinetic data obtained by titration of supernatant. Full symbols represent kinetic data obtained by titration of the $BaTiO_3$ precipitate after removal of the Ti-rich gel phase.

2.4. TEM Observation. The growth of $BaTiO_3$ nanocrystals during the early reaction stages (yield < 2 mol %) could be observed by conventional and high-resolution transmission electron microscopy (TEM and HRTEM) with a JEOL J2010 microscope operated at 200 kV. A precipitation experiment was

performed at 82 °C at a barium concentration of 0.044 mol dm^{-3}. Aliquots of the suspension were collected at different times. The samples were transferred in small bottles and sealed. Immediately before observation, a drop of the suspension was deposited onto a carbon-coated copper grid and dried. Identification of $BaTiO_3$ crystals was carried out using an energy-dispersive electron microprobe and electron diffraction (ED).

3. Results

3.1. Reaction Kinetics. The synthesis conditions are given in Table 1. The Ba/Ti molar ratio in the gel phase at the beginning of reaction (time zero) is practically independent of concentration and equal to 0.64 at 82 °C and 0.55 at 92 °C. The formation kinetics of $BaTiO_3$ is shown in Figure 1. All the curves have a sigmoidal shape and the reaction rate is strongly dependent on concentration. At 82 °C (Figure 1a), as the barium concentration is increased by a factor 2 (from 0.035 to 0.07 mol dm^{-3}), the half-transformation time, $t_{1/2}$, decreases by a factor 70 (from 185 to 2.6 min). At 92 °C (Figure 1b), the reaction is ≈20 times faster at [Ba] = 0.041 mol dm^{-3} than at [Ba] = 0.023 mol dm^{-3}. The effect of temperature can be illustrated by comparing the two experiments (1 and 10) performed at a barium concentration of 0.035 mol dm^{-3}. As the temperature is lowered from 92 to 82 °C, $t_{1/2}$ increases by a factor 30 (from 6 to 185 min). The strong slowing down of the crystallization kinetics induced by a 10 °C decrease of temperature explains why formation of $BaTiO_3$ is not observed near room temperature. At low concentration, the precipitation of $BaTiO_3$ is not quantitative, even after times much longer than the half-transformation time (see Table 1, expts 1, 8, 9). At the highest concentration for both temperatures (expts 5 and 12), formation of $BaTiO_3$ is rather fast and the reaction has already started before the temperature attained the preset value. The corresponding kinetic data were thus discarded. The influence of the [Ba]/[Ti] ratio on the crystallization of $BaTiO_3$ at 82 °C is shown in Figure 1c. The experiments were conducted at a constant Ti concentration of 0.039 mol dm^{-3}. It can be observed that upon increasing R from 1.11 to 1.2, $t_{1/2}$ decreases from 47.5 to 4.5 min. This is a significant effect considering that the barium concentration only changes by 7%.

3.2. Characterization of Final Particles: Morphology, PSD, and Crystallite Size. Mean particle size, size distribution, crystallite size, and equivalent BET diameter of powders vary with temperature, concentration, and Ba/Ti ratio. Figure 2 shows the influence of concentration on the morphology of particles obtained at 82 °C. When [Ba] > 0.04 mol dm^{-3}, spheroidal and reasonably uniform particles are formed. The particle size gradually decreases from 0.86 to 0.36 μm with increasing concentration. It is also evident from Figure 2b−d that the precipitates of $BaTiO_3$ consist of nanosized subunits. In particular, at a barium concentration of 0.044 mol dm^{-3}, the subunits show a pronounced development of facets. At the lowest investigated concentration (0.035 mol dm^{-3}, Figure 2a), in addition to a pronounced faceting, the particles show the tendency to develop a dendritic-like morphology, even if they remain essentially equiaxed. The existence of a substructure is confirmed by the comparison (Table 1) between the average particle size measured by SEM and the XRD crystallite size: d_{50} is 2−4 times larger than d_{XRD}. In turn, the values of d_{XRD} are roughly comparable with the equivalent BET diameters (Table 1), indicating that a significant fraction of the crystallite surface is still accessible to the nitrogen molecules. This can be explained by assuming the existence of a limited number of contact points at the interface between two crystallites, even when the crystallite is part of a polycrystalline assembly. Powders produced at 92 °C show a similar morphology evolution with concentration and the same kind of nanosized substructure. Even at 92 °C, formation of particles with dendritic-like morphology is observed at the lowest concentration investigated (0.023 mol dm^{-3}). For a given barium concentration, the powder obtained at 92 °C is finer (by a factor 1.5−2) than the powder produced at 82 °C (Table 1). The same trend is also exhibited by d_{XRD} and d_{BET}; i.e. the crystallite size decreases with increasing temperature.

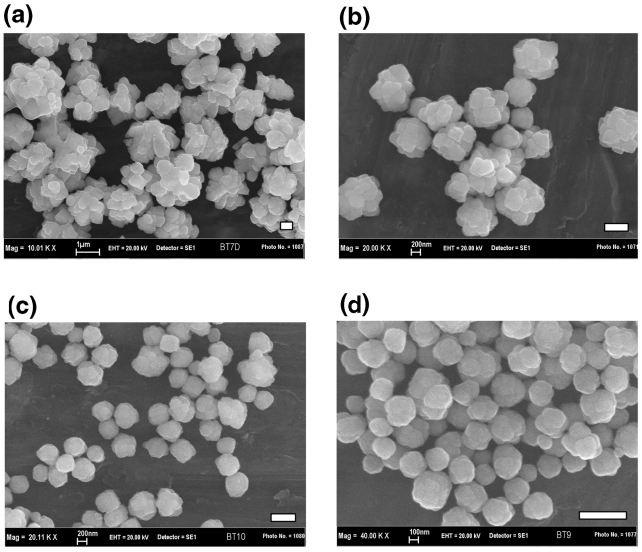

Figure 2. SEM images of $BaTiO_3$ particles obtained at 82 °C: (a) [Ba] = 0.035 mol dm^{-3}, (b) [Ba] = 0.044 mol dm^{-3}, (c) [Ba] = 0.052 mol dm^{-3}, and (d) [Ba] = 0.070 mol dm^{-3}. Bar: 0.5 μm.

3.3. TEM Observation of Early Crystallization Stages. Samples taken after 1, 4, 8, 11, and 15 min during a synthesis carried out at 82 °C and [Ba] = 0.044 mol dm^{-3} were examined. According to Figure 1a, the degree of conversion is <2 mol %, even for the sample reacted for 15 min. Observation of the gel phase did not show distinct particles but rather a continuous matrix without peculiar morphological features. ED and high-resolution observation revealed no evidence of crystallinity. The gel is highly porous with pores and channels which give a very high surface area in contact with the solution. Crystalline $BaTiO_3$ particles were detected only in samples taken at times ≥4 min, as shown in Figure 3. The morphology of the perovskite precipitates in the 4 min sample corresponds to nanosized (5−30 nm) spherical single crystals embedded in the gel phase (Figure 3a). The number of these nanocrystals was quite small, meaning that the extent of conversion is far below 1 mol %. Nanocrystals of 5−30 nm with the same morphology of Figure 3a were observed in all samples, meaning that nucleation continues over a rather long time period. The progressive growth of the primary

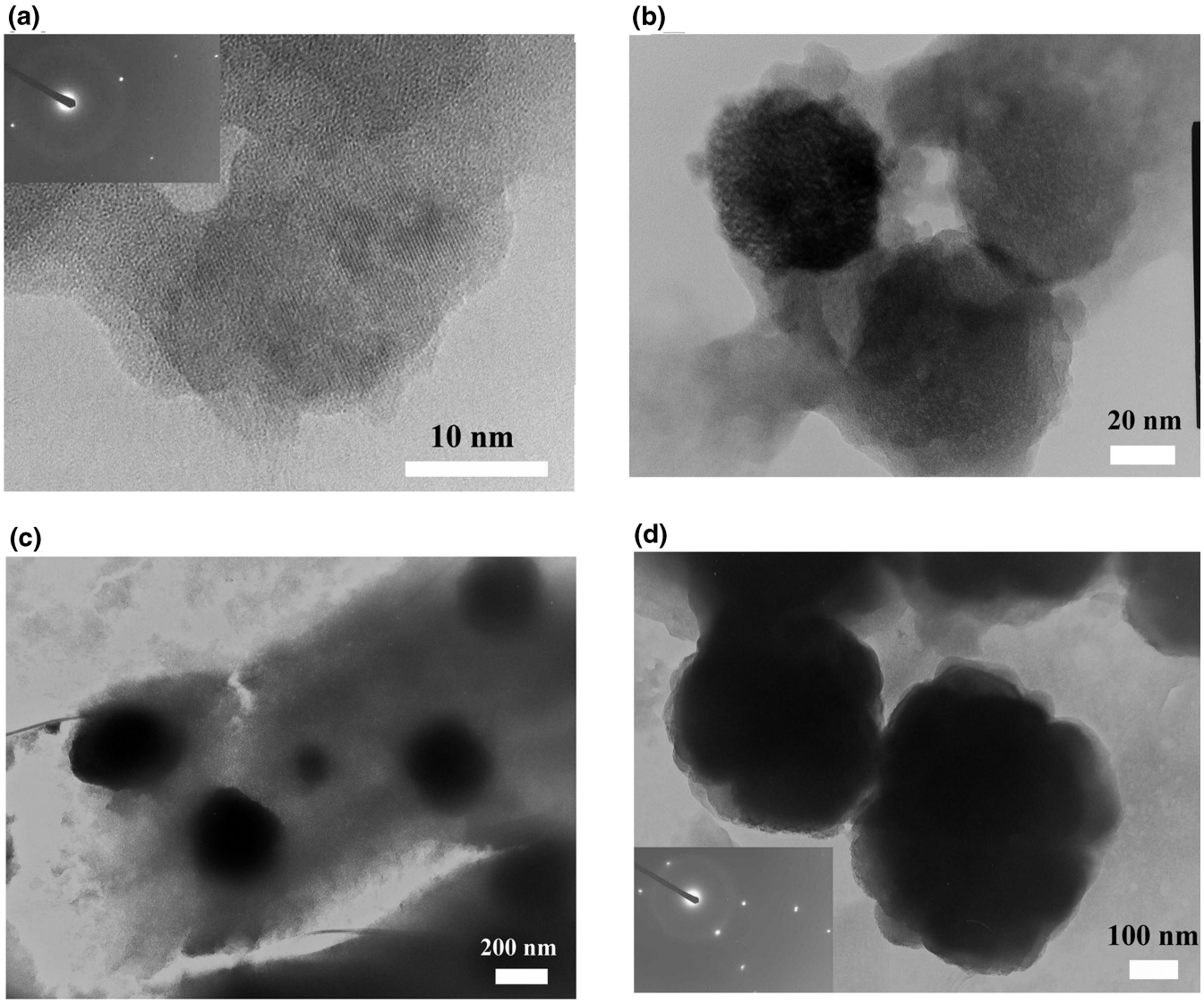

Figure 3. TEM images of the $BaTiO_3$ particles obtained at 82 °C and [Ba] = 0.044 mol dm^{-3}. The precipitate was collected after (a) 4 min, (b) 8 min, and (c,d) 15 min. The continuous phase around the particles is the Ti-rich gel. The inset of parts a and d shows the ED pattern.

$BaTiO_3$ nanocrystals is evident in the samples taken after 8−15 min (Figure 3b,c). For the 8 min sample, particles have grown up to 60−70 nm. Observation in the high-resolution mode has shown that the majority of particles are single crystals, but some are made of two or three crystallites. Further growth of the primary crystals occurred in the sample reacted for 15 min (Figure 3c), where particles of 100−200 nm with smooth surface can be seen. The 15 min sample displays also a different kind of morphology, corresponding to larger particles, up to 500−600 nm, with a rough surface ("raspberry"-like particles, Figure 3d). ED from one of these particles shows reflections 110, 111, 220, and 222 (see inset of Figure 3d). Unlike the ED patterns recorded on smaller particles (Figure 3a), the spots are rather diffuse, and those corresponding to 220 and 222 reflections are split in two. This suggests that the electron beam interacted with multiple $BaTiO_3$ crystals of similar but not identical orientation. However, a detailed investigation on the relative orientation of the crystallites inside the polycrystalline aggregates was not performed.

3.4. Evolution of Crystallite Size and Particle Size. The results of the crystallite size measurements against time for syntheses carried out at 82 °C are presented in Figure 4. A non-negligible growth can be noticed even when transformation is complete. The variation of the mean particle size with time is shown in Figure 5. At a given concentration, the growth rate decreases with time, and for [Ba] ≥ 0.044 mol dm^{-3}, the size only slightly increases once the maximum yield has been attained. Only at the lowest concentration, 0.035 mol dm^{-3}, does particle growth continue after reaction completion. Similar trends were observed at 92 °C. The average number of crystallites per particle, n_c, can be approximately calculated by assuming spherical particles without internal porosity. It turns out that n_c decreases rapidly with increasing concentration. At 82 °C and yield ≈90%, n_c decreases from ≈100 to ≈10 as the concentration increases from 0.035 to 0.070 mol dm^{-3}. The cumulative PSDs of particles collected at various yield values are shown in Figure 6 for two different experimental conditions. The fraction of particles with diameter comparable to the average crystal-

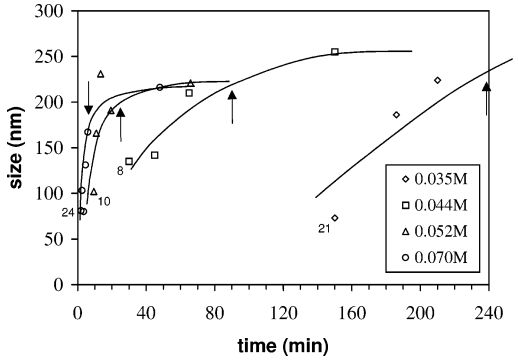

Figure 4. Mean crystallite size (from 111 X-ray line broadening) of $BaTiO_3$ precipitates obtained at 82 °C. The barium concentration is shown in the legend. The number near some data points indicates the yield of the reaction (mol %). The arrows define the time corresponding to completion of precipitation.

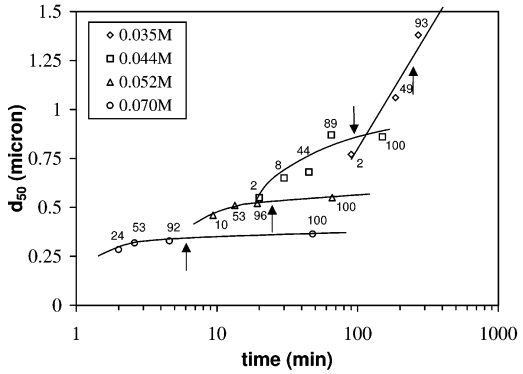

Figure 5. Mean particle size (median diameter of the number particle size distribution) of $BaTiO_3$ precipitates obtained at 82 °C. The barium concentration is shown in the legend. The number near each data point indicates the yield of the reaction (mol %). The arrows define the time corresponding to completion of precipitation.

lite size (Table 1) is quite small, even for low yield values. The dispersion of particle diameter is appreciably broader for the powders obtained at the end of reaction. Accordingly, the difference $d_{90} - d_{10}$ increases from 0.45 to 0.65 μm in Figure 6a and from 0.30 to 0.47 in Figure 6b. It is also worth noting that the span of the PSD, given as $(d_{90} - d_{10})/d_{50}$, strongly increases with decreasing concentration, as shown in Table 1. Combining the kinetic data of Figure 1 with the PSD measurements, the number density of particles was computed, and the results are shown in Figure 7. At the lower concentrations for both temperatures, the number density reaches a maximum or a plateau before precipitation has come to completion. On the contrary, at higher concentration, the curves reach the plateau when the yield of reaction is close to 100%.

4. Discussion

4.1. General Considerations on Crystallization Mechanism. The first stage of the synthesis is the formation of the amorphous Ti-rich gel phase (in the following denoted as BaTi-gel) at room temperature. It is well-known that aqueous solutions of Ti salts, by hydrolysis and condensation reactions, lead to the formation of gels composed of entangled networks of polymeric chains of Ti hydroxides.[15,25] The skeleton of

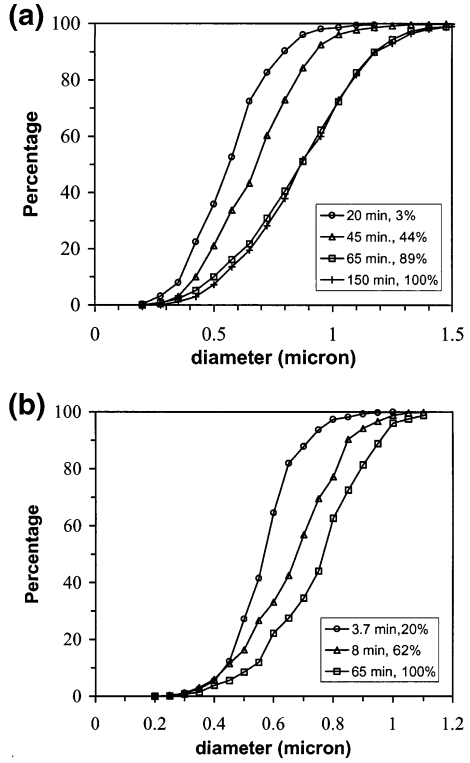

Figure 6. Evolution of the PSD of $BaTiO_3$ particles obtained at (a) 82 °C and [Ba] = 0.044 mol dm^{-3} and (b) 92 °C and [Ba] = 0.029 mol dm^{-3}. The particles were collected at different yield values, as indicated in the legend.

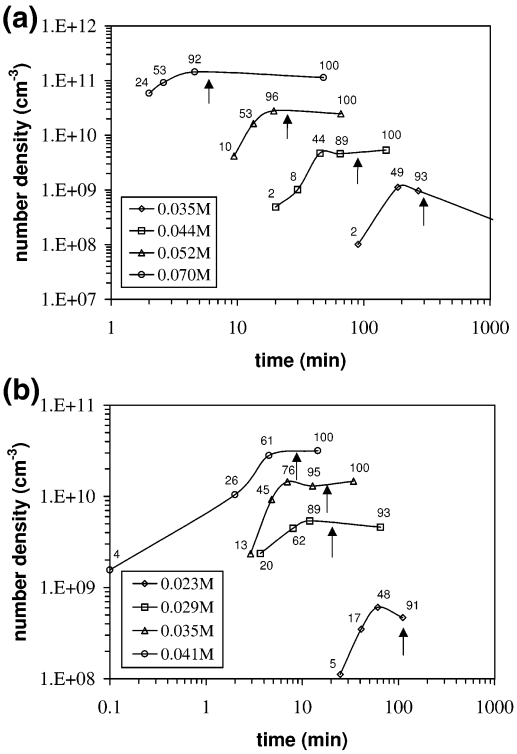

Figure 7. Number density of $BaTiO_3$ particles obtained at (a) 82 °C and (b) 92 °C. The barium concentration is shown in the legend. The number near each data point indicates the yield of the reaction (mol %). The arrows define the time corresponding to completion of precipitation.

the polymer corresponds to Ti atoms linked by bridging O atoms. Since Ba ions do not belong to gel-forming ions, mixed BaTi-gels consist of the skeleton of polymer with

Ba^{2+} ions adsorbed at the surface.[15] The lack of distinct particles and of crystalline features, as shown by HRTEM observation, suggests that the viscous gelatinous suspension initially obtained has a similar structure. The second stage of synthesis is the crystallization of $BaTiO_3$ induced by heating. At room temperature, formation of $BaTiO_3$, although possible from the thermodynamic point of view,[3] is not observed, even after very long times, in agreement with ref 24. The results presented in the previous section strongly indicate that formation of $BaTiO_3$ is dominated by a nucleation and growth mechanism. Therefore, the crystallization process can be represented by the reaction

$$Ba_{sol} + Ti_{sol} + nOH^-(aq) \rightarrow BaTiO_3(s) + mH_2O(l) \quad (2)$$

where Ba_{sol} and Ti_{sol} denote the aqueous species involved in the formation of critical nuclei and successive growth. Since an excess of barium was always used and the BaTi-gel is enriched in Ti in comparison to the 1:1 stoichiometry, barium is readily available as aqueous species. The predominant barium species in solution are Ba^{2+} and $BaOH^+$.[3] On the contrary, the titanium aqueous species implicated in reaction 2 must be provided by dissolution of the BaTi-gel phase:

$$\text{BaTi-gel} + H_2O \rightarrow uTi_{sol} + vBa_{sol} \quad (3)$$

Reaction 3 can occur, for example, by the nucleophilic attack of the hydroxyl ion (which acts as a catalyst) on the terminal Ti atom of the polymeric chains.[25] The solubility of rutile TiO_2 in alkaline conditions is very low. According to the thermodynamic calculations of Lencka and Riman, the predominant titanium aqueous species in equilibrium with rutile at pH > 4 is $Ti(OH)_4$, and its predicted concentration at 25−90 °C is on the order of 10^{-8} mol dm^{-3}.[3,13] The ion $HTiO_3^-$ could also become important under the severe alkaline conditions adopted in the present work. It is expected that the solubility of the gel is higher than that of TiO_2, but in any case probably less than 10^{-6} mol dm^{-3}, as ICP spectroscopy did not reveal an appreciable solubility at room temperature. The lack of an appreciable solubility of TiO_2 in a 1 M solution of $Ba(OH)_2$ at 90 °C has been also reported by Eckert et al.[13] The driving force for reaction 2 is provided by the supersaturation. The supersaturation can be defined as the ratio between the product of the current concentration of the relevant aqueous species and the solubility product of $BaTiO_3$. Basically, this latter equilibrium quantity can be computed from the available thermodynamic data.[3] On the contrary, the concentration of the aqueous titanium species is related to the solubility of the BaTi-gel. Being this latter unknown, the calculation of supersaturation is precluded. Nevertheless, the concentration of the titanium aqueous species, at least at the beginning of reaction, will be nearly constant, because of the presence of the BaTi-gel phase. Since the pH is also approximately constant, the initial variation of supersaturation will be mainly related to the variation of barium concentration in solution, as suggested by Figure 1c.

4.2. Primary and Secondary Nucleation. The initial, low crystallization rate is likely to be controlled by the rate of primary nucleation. For primary nucleation we intend nucleation in the absence of preexisting crystalline matter. As often occurs, it is impossible to decide whether initial nucleation is predominantly homogeneous or heterogeneous. TEM observation of early (yield < 1%) crystallization stages (Figure 3) has shown that the formation of an appreciable number of primary nanocrystals in the range 5−30 nm requires a non-negligible time in comparison to the half-transformation time. This provides evidence that primary nucleation is quite slow. Observation of the particle morphology (Figures 2) and comparison among crystallite size (Figure 4, Table 1), BET equivalent diameter (Table 1), and average particle size (Figure 5, Table 1) clearly indicates that the $BaTiO_3$ precipitates obtained under the different experimental conditions are composed of polycrystalline particles. The polycrystalline morphology is already observed for yield values on the order of a few percent and then retained until reaction completion. Basically, polycrystalline particles can be originated by two different mechanisms: secondary nucleation at (or in the vicinity of) the surface of already existing crystals or colloidal aggregation of smaller units.[9−10,25] However, the colloidal aggregation process has no influence on the overall degree of conversion. Consequently, the upward curvature and the dramatic increase of the reaction rate (typically 1 order of magnitude moving from ≈0 to 20% yield) can be hardly explained by considering only primary nucleation, growth, and aggregation of primary particles. On the contrary, secondary nucleation can easily account for the acceleration of the reaction kinetics. At the very beginning, primary nucleation leads to formation of supercritical nuclei that grow further. Since the rate of secondary nucleation is proportional to the total surface of available particles, it will increase very rapidly after an initial period of time, like in a self-catalytic process. Obviously, at a later time, the lowering of supersaturation will induce a decrease of secondary nucleation rate and growth will become predominant. As a result, each single nanocrystal of $BaTiO_3$ generated at the beginning of reaction by primary nucleation can lead to a distinct final polycrystalline particle by a succession of secondary nucleation events and growth of the resulting crystallites.

Secondary nucleation at (or in the vicinity of) the surface of particles already present in solution is rather common and can have a large influence on crystallization,[26] although relatively few examples have been described in the recent literature. Hydrothermal synthesis of polycrystalline, faceted $PbTiO_3$ particles composed of multiple crystallites with slightly different orientation by a process of secondary nucleation and growth has been described by Peterson and Slamovich.[27] Significant changes in size and morphology of portlandite (calcium hydroxide) crystals upon aging of aqueous suspensions have been attributed to a similar process.[28] Secondary nucleation has been also invoked

(25) Brinker, C. J.; Scherer, G.W. *Sol−Gel Science. The Physics and Chemistry of Sol−Gel Processing*; Academic Press: San Diego, CA, 1990.

(26) Mullin, J. W. *Crystallisation*; Butterworths: London, 1972.

(27) Peterson, C. R.; Slamovich, E. B. *J. Am. Ceram. Soc.* **1999**, *82*, 1702.

(28) Rodriquez-Navarro, C.; Hansen, E.; Ginell, W. S. *J. Am. Ceram. Soc.* **1998**, *81*, 3032.

to explain the development of polycrystalline particles with unusual morphologies or complex structures.[29−31]

4.3. Growth. The number density of particles remains almost constant or even decreases once the degree of transformation exceeds 50% (see Figure 7). This is an indication that the second stage of reaction is dominated by the growth of the crystallites nucleated (and grown to some extent) during the first stage. Likely, the crystals at the surface of the aggregates grow much faster than those in the interior, because they have surfaces directly exposed to solvent. However, the results of BET measurements (Table 1) suggest that the solvent and the aqueous species involved in growth can have access to a fraction of the inner surfaces of the aggregate, and therefore, a solvent-mediated recrystallization process of the whole aggregate cannot be excluded. It is well-known that a variation of supersaturation can induce a modification of crystal habit, because the growth rate of different surfaces can be differently influenced by concentration.[9] Previous studies on the synthesis of $BaTiO_3$ from $Ba(OH)_2$ solutions at 90 °C reported a variation of particle morphology from spherical or cubic to octahedral with decreasing concentration.[20,22] Thus, the tendency to develop dendritic-like morphologies at low concentration (Figure 2) can be possibly ascribed to preferential growth along some directions or preferred secondary nucleation on specific faces.

All the experiments are well-represented by a single master straight line if the logarithm of particle size at the end of reaction is plotted against the logarithm of the maximum reaction rate (i.e. the maximum slope of the kinetic curves of Figure 1), as illustrated in Figure 8. The maximum reaction rate is always located close to 50% conversion. As discussed in the foregoing paragraph, the reaction rate at this stage is mainly related to the growth process. The location of the different data points reveals that higher reaction rates and smaller particles correspond to higher values of temperature, concentration, and Ba/Ti ratio. This suggests that an increase of the above factors produces a rise of supersaturation, which leads to an increase of the nucleation rate during the initial reaction stage.

The observed rapid decrease of the number of crystallites per particle and the concomitant increase of the number density of particles strongly indicates that the primary nucleation rate increases faster than the secondary nucleation rate with increasing supersaturation. This corresponds to a larger number of smaller particles (see Figure 7) and faster transformation when the stage of predominant growth is reached. For example, at 82 °C, as the concentration increases from 0.035 to 0.070 mol dm^{-3}, the number density of particles increases ≈2 orders of magnitude and the total surface of the particles increases ≈1 order of magnitude.

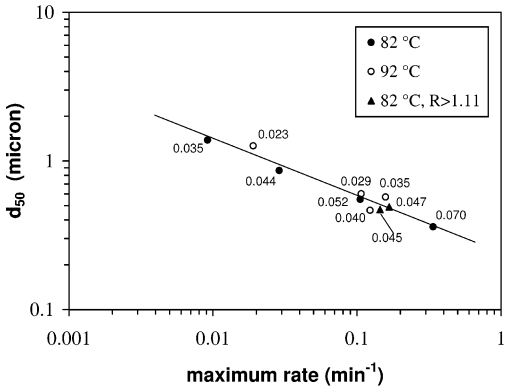

Figure 8. Diameter of $BaTiO_3$ particles against the maximum reaction rate obtained from Figure 1. The number near each data point indicates the barium concentration (mol dm^{-3}).

The growth of both the crystallites (Figure 4) and the particles (Figure 5) is not completely arrested, even when the transformation is complete, indicating an Ostwald-like ripening process related to dissolution of the smallest crystallites and coarsening of the largest. At high concentration, recrystallization is mainly confined within the particles. At lower concentration (0.035 mol dm^{-3} at 82 °C and 0.023 mol dm^{-3} at 92 °C), a significant decrease of the number density of particles can be noticed (Figure 7). In these cases, the ripening process leads to the disappearance of entire classes of particles on the left-hand side (lower dimension) of the PSD and appearance of new classes on the right-hand side. As a result, the width of the distribution increases. For the synthesis carried out at 82 °C and at barium concentration of 0.035 mol dm^{-3}, the difference $d_{90} - d_{10}$ increases from 1.6 after 4.5 h aging to 2.2 after 22 h aging, while the yield remains constant (92%). This notable effect is, at least in part, related to the very long aging time adopted.

Acknowledgment. This work has been funded, in part, by the European Community under the "Competitive and Sustainable Growth" Program, contract no. G5RD-CT-1999-00123. The authors wish to thank Mr. C. Uliana and the Department of Chemistry and Industrial Chemistry, University of Genoa, for TEM observation.

CM031130K

(29) Cölfen, H.; Qi, L.; Mastai, Y.; Börger, L. *Crystal Growth Design* **2002**, *2*, 191. (b) Qi, L.; Cölfen, H.; Antonietti, M.; Li, M.; Hopwood, J. D.; Ashley, A. J.; Mann, S. *Chem. Eur. J.* **2001**, *7*, 3526.

(30) Busch, S.; Dolhaine, H.; DuChesne, A.; Heinz, S.; Hochrein, O.; Laeri, F.; Podebrad, O.; Vietze, U.; Weiland, T.; Kniep, R. *Eur. J. Inorg. Chem.* **1999**, 1643.

(31) Cölfen, H.; Qi, L. *Chem. Eur. J.* **2001**, *7*, 106.